

Seismic surface waves in a suburban environment: Active and passive interferometric methods

DAVID HALLIDAY and ANDREW CURTIS, University of Edinburgh, UK
ED KRAGH, Schlumberger, Cambridge, UK

Seismic interferometry refers to a new range of methods where inter-receiver wavefields (those that would have been recorded if one of each pair of receivers had been a source) can be estimated by cross-correlation of wavefields recorded at each of the receivers. These methods have found many applications in different fields of seismology, including creating “virtual” sources in wells under complex overburdens, computational full-wavefield modelling, and passive construction of surface wave waveforms from background noise in the Earth. Curtis et al. (2006) provide an overview of various applications of seismic interferometry referred to herein, and more in-depth works can be found in the special supplement on Seismic Interferometry in the July-August issue of *GEOPHYSICS*.

One particularly interesting aspect of seismic interferometry is the ability to estimate inter-receiver signals using background noise. This has become popular for crustal-scale imaging where crustal and uppermost mantle structure can be constrained using surface wave velocity analysis. However, successful applications of similar methods to higher-frequency data are scarce. One application is presented by Draganov et al. (2007), who use long recordings of noise (around 10 hours) to recover both surface waves and reflected body waves in a hydrocarbon exploration, desert setting.

This article will focus on surface-wave construction and isolation and is not restricted to passive noise sources; active sources have also been used to successfully isolate higher frequency, inter-receiver surface waves. For example, direct surface waves determined in this way have been used as part of a predictive ground roll removal algorithm in an exploration setting (Curtis et al., 2006; Dong et al., 2006; Halliday et al., 2007).

In the civil engineering community, there are existing methods that extract near-surface information from background noise, known as “micro-tremor analysis.” For example, the spatial autocorrelation method (SPAC) of Aki (1957) extracts phase velocities from recordings of background noise, while Louie (2001) uses the refraction micro-tremor technique to resolve velocity structure to depths of 100 m using slowness-frequency analysis of background noise. The advantages of such methods are the low cost and manpower in the data acquisition compared with active source surveys, and the fact that noisy (sub-)urban settings in which the data are often acquired are ideal for the application of methods of noise analysis. Since the same type of data are used for passive interferometry, the same advantages apply. For example, Chávez-García and Luzón (2005) compare and contrast the analysis of micro-tremor measurements using the SPAC method and the passive interferometric method and found that the two methods provide complementary results.

In this study, we show results of several different approaches to the interferometric estimation of surface waves in a suburban environment, using both active and passive sources. For the active source case, we illustrate that multimode surface waves can be estimated robustly using specific source geometries that suppress body wave arrivals.

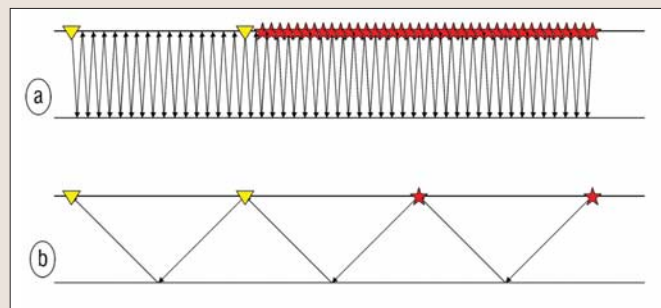


Figure 1. (a) For the guided wave between two receivers in this two-layer model, stationary points exist at all offsets on an extension of the inter-receiver line. (b) For a singly reflected wave, stationary points exist only at offsets equal to the receiver separation.

We also show that surface wave gathers from a line of shots can be estimated at a fraction of the cost using interferometry. Further, we find that in this specific application that the interferometric estimates have a wider range of dominant frequencies due to differences in the receiver types used. These estimates have applications in deep seismic surveys, where surface waves are treated as noise and the estimates can be used as part of the aforementioned ground-roll removal methods. There are also potential applications in near-surface geophysics as the interferometric estimates may provide a cheap alternative for the acquisition of densely sampled surface-wave data, from which near-surface velocity profiles can be extracted (e.g. Roth and Holliger, 1999; Park et al., 2007).

For the passive case, we illustrate that surface wave estimates can be produced using interferometry and that the quality of these estimates can be enhanced with some simple filtering steps. These steps account for the adverse effects of directional bias in the noise and the short recording periods used. To take full advantage of the noise in this setting, we conclude that it may be beneficial to account for known sources of noise during survey planning.

The passive estimates occupy a lower frequency range than both the directly recorded data and the active source interferometric estimates. A combination of these different approaches may therefore allow a wider frequency range to be covered, allowing a greater range of depths to be studied with the data.

Surface wave estimation. In theory, seismic interferometry between a pair of receivers requires that either noise or active wavefield sources (both point force and deformation rate tensor sources—henceforth referred to as *background* sources) span a boundary that totally encloses a volume of the Earth that includes both of the receiver locations of interest. In this configuration, the full inter-receiver wavefield is determined by calculating a so-called interferometric integral that includes cross-correlations and summations of the recordings at each receiver (Wapenaar and Fokkema, 2006). In practice, active background sources cannot be located so as to span an enclosing boundary completely and this affects our ability to estimate the inter-receiver signals accurately. Snieder et al. (2006) illustrate the resulting errors incurred

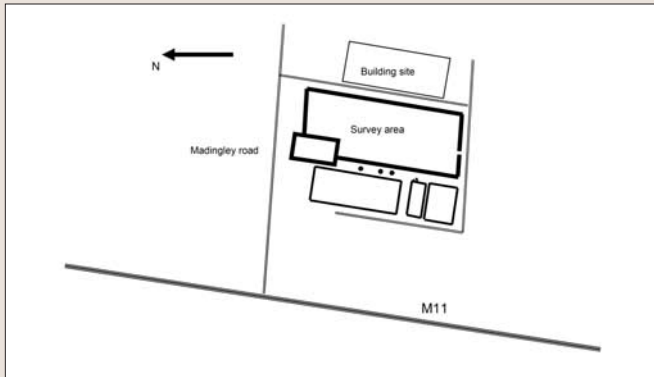


Figure 2. Sketch map of the survey area. Major sources of background noise are the M11 (a busy motorway), Madingley Road (a main route into Cambridge) and a Building site to the east of the survey area.



Figure 3. Looking north from the southeast corner of the survey area, showing wacker operation, with Schlumberger Cambridge Research in the background.

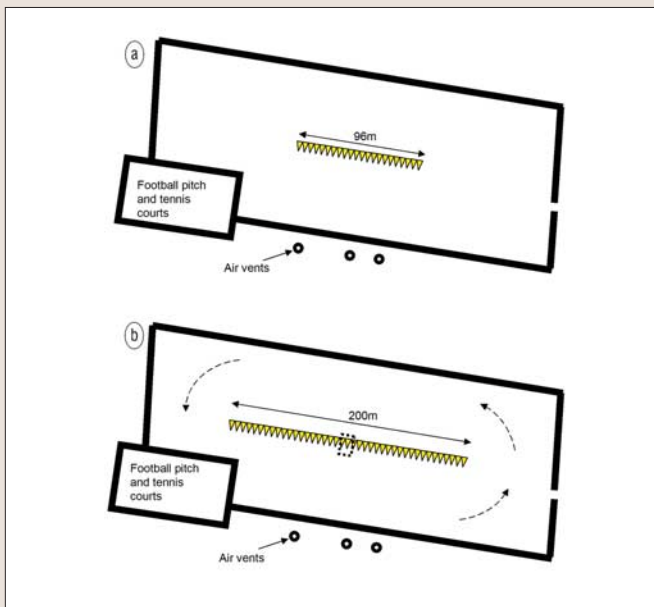


Figure 4. (a) Sketch of the location of the 96 m line of co-incident source and receivers within the survey area. Locations are numbered 1 to 96 from north to south. (b) Sketch of the location of the 200 m line of coincident sources and receivers. Dashed box illustrates the 7×8 geophone grid. Dashed arrows indicated direction of motion of the family saloon car.

for direct and reflected waves by analyzing stationary phase locations for the inter-receiver wavefield (a location where a background source provides a dominant contribution to a certain part of the constructed wavefield). Sabra et al. (2005) use a similar approach to that of Snieder et al. (2006) and consider the case of a simple acoustic guided wave (similar to the elastic surface waves considered here, which are formed by the interference of many high-order, free-surface multiples). This approach shows that for a guided (surface) wave, stationary points are those at which a source would produce a packet of energy that would pass (and be recorded by) one receiver of the pair, and then, the *same* packet of energy would pass through the other. In a horizontally-layered Earth, these would exist at locations all along an extension of the inter-receiver line (Figure 1a), while primary reflected wave stationary points only exist at offsets equal to integer multiples of the receiver separation (Figure 1b). We define two regions of stationary points: one at short offsets (offsets less than the receiver separation) where there are predominantly stationary points for the surface waves, and one at longer offsets (those offsets equal to and greater than the receiver separation) where we may expect stationary points for all types of arrivals.

By restricting background active sources to the extension of the inter-receiver line, we expect the inter-receiver estimate is dominated by direct surface waves, since these are stimulated by many more stationary points than are the body waves (see Halliday et al., 2007; also, Figure 1). A similar argument can be used for the passive case, i.e. when passive noise sources are predominantly located at or near the surface of the Earth, they are more likely to contribute inter-receiver surface waves than body waves.

For active sources, we can write the interferometric integration approximately as a sum over cross-correlations for n source positions (cf. Equation 1 of Bakulin and Calvert, 2004), i.e.

$$g_{33}^{est}(x_A, x_B, t) + g_{33}^{est}(x_A, x_B, -t) = \sum_n g_{33}(x_A, x_n, t) * g_{33}(x_B, x_n, -t). \quad (1)$$

Here $g_{33}(x_A, x_B, t)$ is the Green's function representing the vertical component of particle velocity at x_A due to a vertical point force at x_n (a Green's function is a mathematical representation of the interpoint wavefield arising from an impulsive point source), the superscript *est* indicates that this is an estimate of the Green's function, and "*" denotes convolution. We assume that vertical components dominate the recordings and hence do not consider horizontal components. Note that the Green's function on the left of Equation 1 consists of a sum of a causal Green's function and an acausal Green's function. The recovery of both of these Green's functions is dependent on having sources, x_n , on both sides of the receiver pair.

For passive sources we write the interferometric construction as a sum over cross-correlations for n time windows, i.e.

$$g_{ik}^{est}(x_A, x_B, t) + g_{ik}^{est}(x_A, x_B, -t) = \frac{1}{|S(\omega)|^2} \sum_n v_i^{obs}(x_A, t_n) * v_k^{obs}(x_B, -t_n). \quad (2)$$

Here $v_i^{obs}(x_A, t_n)$ is the i th component of particle velocity at x_A due to a distribution of random noise sources, recorded for a time window t_n and $|S(\omega)|^2$ is the power spectrum of the excitation. Wapenaar and Fokkema (2006) discuss in detail the assumptions required in expressions such as 1 and 2

above, but applications like the subsurface virtual source work of Bakulin and Calvert (2004) show that some of these assumptions, particularly with respect to source geometry, can be relaxed with still useful results.

Data acquisition. In this study, we use three different but complementary data sets acquired in a field adjacent to the Schlumberger Cambridge Research Center (Cambridge, England). A sketch map of this area, including known sources of background noise is shown in Figure 2.

The first data set is an active source data set consisting of 96 receiver locations with 1-m separation along a straight line, with sources beside each receiver location in turn (Figure 4a). The data were acquired using a wacker vibrator as source (Barbier et al., 1976), with a “sweep” length of around 30 s (acquisition is illustrated in Figure 3). Two geophone types were used: 95 standard 10-Hz vertical component geophones to record the seismic data, and a single damped geophone placed beside each source location in turn to record the source sweep of the vibrator. The latter record can be cross-correlated with all other records to create shot-gathers with a pseudo-impulsive source signature, a typical example of which is shown in Figure 6. Note (a) the shallower body wave arrivals (guided P-waves, 0 to 0.1 s), (b) the more horizontal shallow reflection events (0.1 to 0.2 s), (c) the higher-frequency surface waves, and (d) the less clear lower-frequency surface waves. The equivalent frequency-wavenumber plot is shown in Figure 7. Note that in addition to (a) the fundamental mode, there is (b) one strong higher mode, and (c) at least one other higher mode surface wave. The dominant body waves (d) are clearly separated from the surface waves in this plot.

The second and third data sets were acquired using a second geophone layout: a 200-m line of receivers with 5 m geophone separation, and an additional 7×8 geophone grid located in the center of this line with a grid spacing of 1 m (Figure 4b). Using this geometry we first recorded around 30 minutes of controlled noise (a Skoda Octavia estate family saloon car circling the geophone spread in a spiral motion, Figures 4 and 5) followed by approximately 90 minutes of background, suburban noise (Figure 2 shows known sources of background noise).

Active source interferometry. To estimate the Green’s functions between a pair of receivers, the responses from a series of outer sources (sources on one or both sides of the receiver pair) recorded at both receivers are cross-correlated (that is, the outer sources are used as background sources). Consider the uncorrelated vibrator data, $d_{33}(x_A, x_B, t)$ from a source at location A and a receiver at location B:

$$d_{33}(x_A, x_B, t) = [g_{33}(x_A, x_B, t) * s(t) * r^s(t)] \quad (3)$$

where $g_{33}(x_A, x_B, t)$ is the Green’s function representing the vertical component of particle velocity due to a vertical, impulsive point force source, $s(t)$ is the vibrator source signature, and $r^s(t)$ is the receiver response function of the standard geophone. By using Equation 2 to cross-correlate and sum the uncorrelated data recorded at A and B from n other inline shots, we gain an estimate of the inter-receiver Green’s function

$$\begin{aligned} \hat{g}_{33}^{est}(x_A, x_B, t) &= \\ & \sum_n [g_{33}(x_A, x_n, t) * s(t) * r^s(t)] * [g_{33}(x_B, x_n, -t) * s(-t) * r^s(-t)] \\ &= \sum_n [g_{33}(x_A, x_n, t) * g_{33}(x_B, x_n, -t)] * [s(-t) * s(t)] * [r^s(-t) * r^s(t)] \quad (4) \end{aligned}$$



Figure 5. Looking east across the survey area showing the Skoda ‘passive’ source in action.

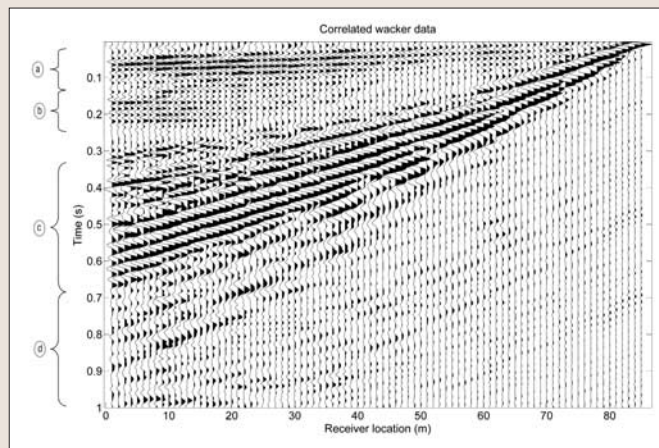


Figure 6. Correlated vibrator gather from a source at location 86. Labels correspond to (a) guided P-waves, (b) shallow P-wave reflections, (c) higher-frequency surface waves, and (d) lower-frequency surface waves.

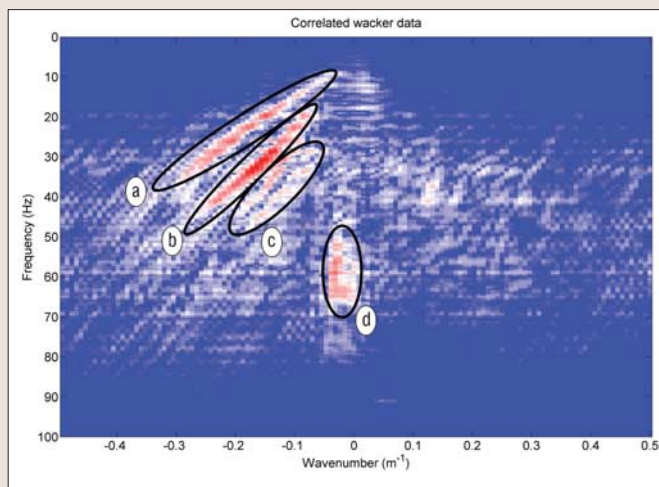


Figure 7. Data shown in Figure 6 plotted in the f-k domain. Labeled areas show the dominant areas of, (a) the fundamental mode surface wave, (b) a strong higher mode surface wave, (c) weaker higher mode surface waves, and (d) the body waves (both guided P-waves and shallow reflected P-waves).

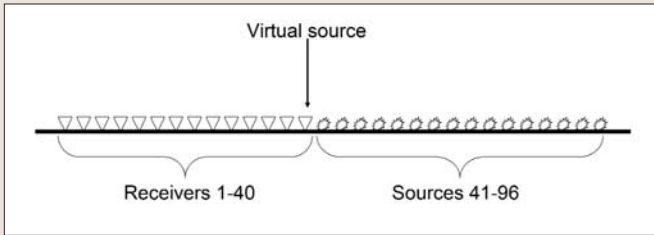


Figure 8. Source and receiver positions used in Figure 9 and Figure 10. Receivers are shown as triangles, sources as flashes.

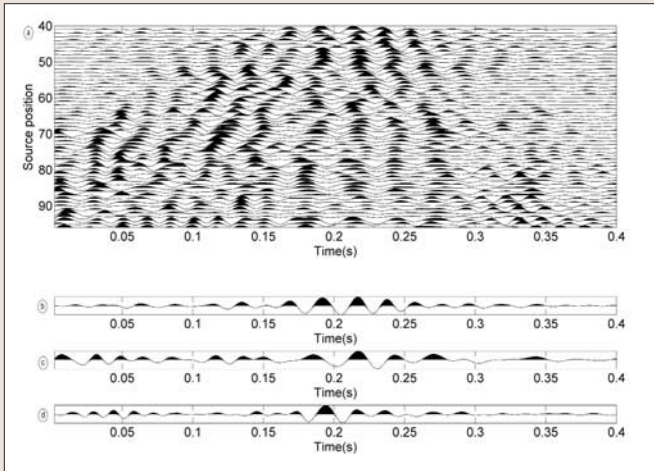


Figure 9. (a) Cross-correlations between receivers 10 and 40 using sources at different locations (see Figure 8); (b) the sum of cross-correlations 44 to 53; (c) the sum of all cross-correlations; (d) true source-receiver data.

where $\hat{g}_{33}^{est}(x_A, x_B, t)$ is the estimated Green's function modified by source signatures and receiver response functions. We replace the Green's function cross-correlation and summation (the first term in square brackets) with the estimated Green's function (Equation 1) and write our modified estimate as

$$\hat{g}_{33}^{est}(x_A, x_B, t) = g_{33}^{est}(x_A, x_B, t) * [s(t) * s(-t)] * [r^s(t) * r^s(-t)] \quad (5)$$

i.e. the estimated signal is equal to the Green's function between receiver A and B modulated by the auto-correlation of the source signature (approximately an impulse at $t = 0$) and the auto-correlation of the receiver response function.

We can then compare this result with that obtained in an actual source-receiver record after correlation with the vibrator source signature:

$$d_{33}(x_A, x_B, t) = g_{33}(x_A, x_B, t) * [s(t) * s(-t)] * [r^d(t) * r^d(-t)] \quad (6)$$

where $r^d(t)$ is the receiver response function of the special damped geophone.

Note the similarities between the shot record in Equation 6 and the interferometric estimate in Equation 5. Differences arise due to the difference in the damped geophone response function and the standard geophone response function. Further differences arise depending on the source and receiver configuration. For example, when we have background sources distributed as described above, then the estimate is dominated by the inter-receiver surface waves.

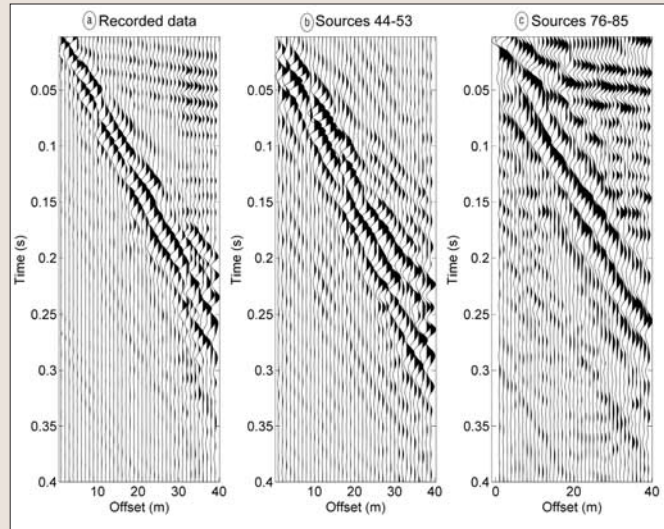


Figure 10. (a) Shot-gather showing surface and body waves, (b) interferometric estimates produced by summing background source locations 44-53, and (c) by summing background source locations 76-85.

Differences also occur due to attenuation: the energy arriving at the first receiver (the virtual source) in the interferometric construction in Equation 5 has already propagated a certain distance; therefore, energy has been lost due to anelastic attenuation, which will not occur when an active source is placed at that point as in Equation 6.

Figure 9d shows the recorded data at receiver 10 (in Figure 8) from a source-receiver record when a source was placed beside the virtual source location at receiver 40. The ground roll can be seen between 0.13 s and 0.28 s. Figure 9a illustrates the cross-correlations of signals recorded at two receivers (numbers 10 and 40) from individual sources at various offsets from (and to the right of) the virtual source at position 40 (for visualization, all traces are normalized to have a peak amplitude of 1). The set of non-normalized records would be summed (Equation 4) to construct an interferometric waveform from a virtual source located at receiver 40, as shown in Figure 9c. We now analyze contributions to the summed waveform in Figure 9c in more detail.

In the region of the ground roll in Figure 9d, there are contributions to the sum from sources at short and long offsets (i.e., these contributions sum positively). Whereas, for other arrivals such as those identified as guided waves and shallow reflections (0 s–0.13 s), contributions exist for background sources at long offsets but do not occur for short offsets (Figure 1).

In Figure 9b, we limit the source array to shorter offsets (up to 20 m): after summation (Equation 4), the surface wave component dominates the result (compare Figures 9b, c, and d). This agrees with the stationary phase argument presented earlier: contributions to the interferometric construction of a surface wave come from both short offsets (i.e., those less than the receiver separation) and long offsets (up to and beyond the receiver separation), while contributions to reflected waves and low-order multiples come from offsets close to and beyond the receiver separation (Halliday et al., 2007).

Figure 10a shows the complete shot gather of sweep-correlated vibrator data from a source placed at receiver location 40 recorded at receivers 1–39. Figure 10b shows the sum of the interferometric cross-correlations for background sources 44–53 (short offsets), and Figure 10c the sum of cross-correlations for background sources 76–85 (offsets

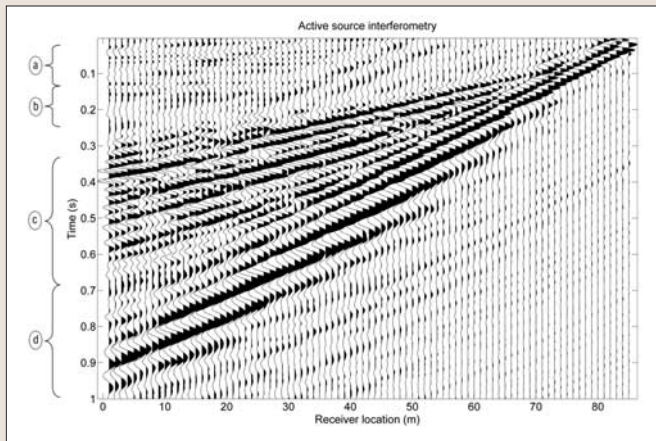


Figure 11. Interferometric estimate for a virtual source at location 86. Background sources used in the estimate are at locations 89–96. Labels correspond to (a) guided P-waves, (b) shallow P-wave reflections, (c) higher-frequency surface waves, and (d) lower frequency surface waves.

around the maximum virtual source/receiver separation). As we expect, the result using sources at near offsets is dominated by surface waves, while the result using the far offsets includes both the surface waves and body waves as predicted. The appearance of the surface-wave train changes across the three parts of Figure 10. These changes are likely to be due to the variation in the source signatures and receiver response functions identified above. As expected, note that the long-offset sources in Figure 10c produce results that are lower frequency than those from near-offset sources due to attenuation.

Figure 11 shows the estimate of the surface waves corresponding to the data shown in Figure 6. Here we have used background sources at locations 89–96 and therefore expect our estimate to be dominated by inter-receiver surface waves (similar to Figure 10b). Compared with Figure 6, we see the estimate is dominated by both (c) the higher-frequency surface waves and (d) the lower-frequency surface waves. Where we expect body waves (a, b), there are no strong arrivals.

The corresponding f - k plot is shown in Figure 12. The same areas indicated in Figure 7 are indicated here, and we can identify (a) the fundamental mode surface wave, (b) the stronger higher mode, and (c) the other higher mode surface waves. As in Figure 11, any body wave arrivals (d) are weak. Note that the different modes occupy larger areas than those in Figure 7 and that there is a broader dominant frequency band. The difference in strength of the surface waves in the interferometric estimate, relative to those in Figure 6 and Figure 7, is likely to be related to the difference between the two types of receiver used, i.e. the differences between Equations 5 and 6 above.

Our results illustrate that by using active source interferometry, we can create high quality estimates of both fundamental and higher mode surface waves. In Figure 11, we have used seven sources to estimate a single shot gather, and the same seven sources can be used to create “virtual” sources at each of the 86 receivers. In other words, we can turn each receiver into a virtual source, but at a fraction of the effort and cost required.

Passive interferometry. Both of the passive data sets are processed in a similar fashion to above: first the data are split into many time windows and one-bit normalized (this stops high-amplitude noise bursts dominating interferometric cross-correlations). For each receiver pair, the corresponding time

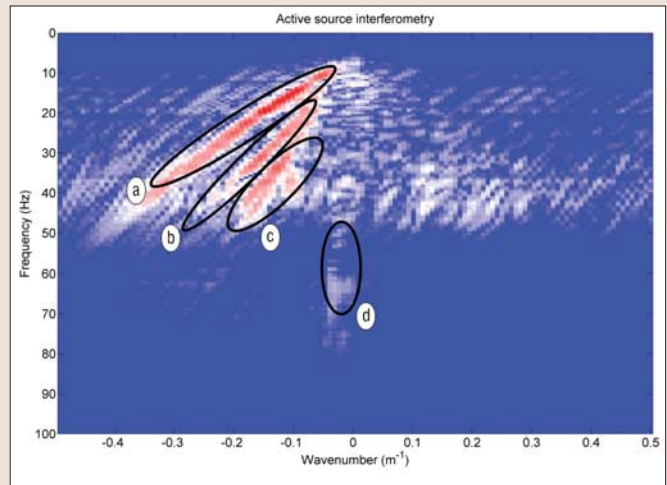


Figure 12. Data shown in Figure 11 plotted in the f - k domain. Labeled areas are the same as those in Figure 7.

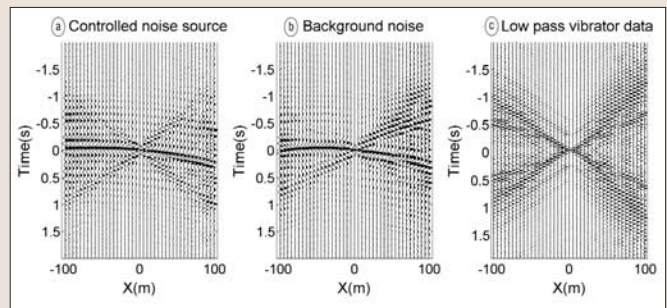


Figure 13. (a) Cross-correlation of controlled noise, (b) cross-correlation of random background noise, (c) and the vibrator data. Both causal and acausal results are shown. $X(m)$ is the source/receiver offset—negative offsets are to the south, with positive offsets to the north.

windows are cross-correlated and the results are integrated over time. We use overlapping time windows of 3 s, as this provides sufficient time for the slowest surface wave to be observed by all receivers within the same time window.

Figures 13a and b show the results of cross-correlating windows of noise recorded from the controlled Skoda noise (around 30 minutes in total) and uncontrolled noise (around 90 minutes in total). Both of these examples are for a “virtual source” in the center of the line. Figure 13c shows the recorded data (reflected about the zero-time axis) for a real source at the same location for comparison. Again, traces are normalized to peak amplitude of 1 prior to plotting. The cross-correlations have lower frequency content (5–15 Hz) than the vibrator data (approximately 10–100 Hz); therefore, we plot the lower frequency part of the vibrator data (10–20 Hz).

Both of the noise results are dominated by a strong spurious event that curves around the zero time axes. We have confirmed that this strong event is due to a stationary source of noise that operated throughout the recording period (a piece of heavy machinery periodically hammering piles into the ground on the building site shown in Figure 2). Nevertheless, the trend of the dispersive surface wave pattern can be seen in some parts of the interferometric estimates. For example, the Skoda data show the same X -pattern of the surface waves. Part of the pattern can also be seen in the background noise data. At positive times, these events can be seen moving out from zero offset to -100 m offset, and for negative times, a similar event can be seen moving out from zero offset to 100 m offset. Note that because we have controlled the location of the Skoda, which circled the receiver array spiralling

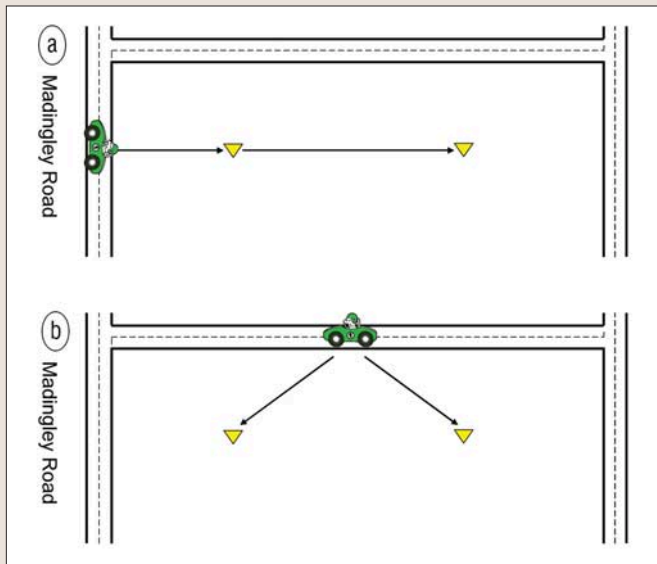


Figure 14. Cartoon illustrating the role of different passive source locations (indicated by a car) relative to receiver locations (triangles). (a) A car (travelling along the busy Madingley Road) passes the extension of the receiver line and emits a packet of seismic noise that travels to the first receiver, is recorded at this receiver and then travels along the inter-receiver path to the second receiver. This packet of noise contributes to the inter-receiver surface wave in the interferometric estimate. (b) A car travels along a road that lies off the receiver line. A packet of noise travels to both the first and second receivers but does not travel along the inter-receiver path. Hence this does not contribute to the interferometric surface-wave estimate, but may contribute spurious energy in the cross-correlations.

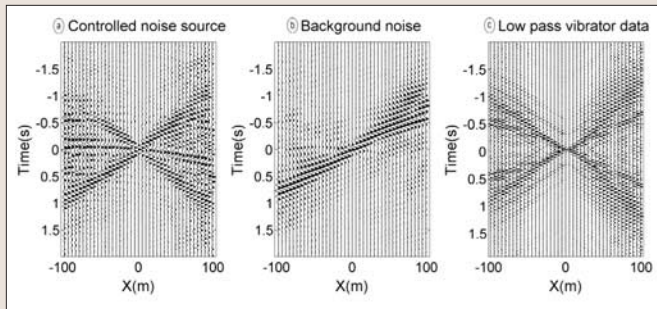


Figure 15. As for Figure 13. Here data have been selected using directional analysis across the 2D array.

inwards, we expect to have noise from all directions; therefore, in (a) we see these arrivals both upline (from 0 to 100 m), downline (from 0 to -100 m), and at both positive and negative times, i.e. we have estimated both causal and acausal Green's functions (Equation 2). Traffic on Madingley Road dominated the recordings of background noise used in (b), and due to this bias in noise directionality, we do not expect to have the same coverage of source locations; hence, the less complete surface wave pattern.

Since the estimates are dominated by the strong spurious event, we take action to reduce its effect, in order to extract better surface wave estimates. A simple process to extract the inter-receiver surface waves is to use a beam-forming method on the small array in the middle of the 200 m line (Figure 4). Using this approach, we can detect and isolate noise coming from certain directions, e.g. from the direction of either end of the line where we expect the majority of stationary points contributing to the direct inter-receiver surface waves to be located (Snieder, 2004; Figure 14). We refer to this process as target-orientated passive interferometry. In this case, our "target" is the direct-surface wave (borrowing the terminology of

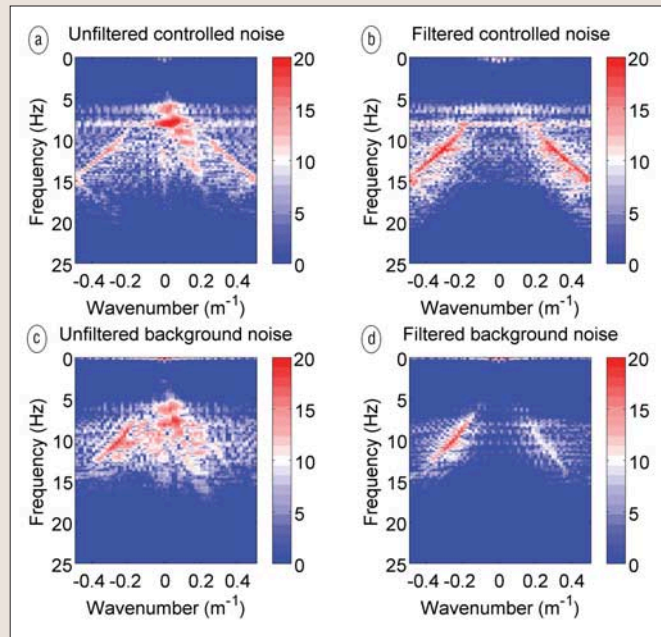


Figure 16. *f-k* plots for (a) controlled noise interferometric data, (b) *f-k* filtered controlled noise interferometric data, (c) unfiltered background noise interferometric data, and (d) *f-k* filtered background noise interferometric data.

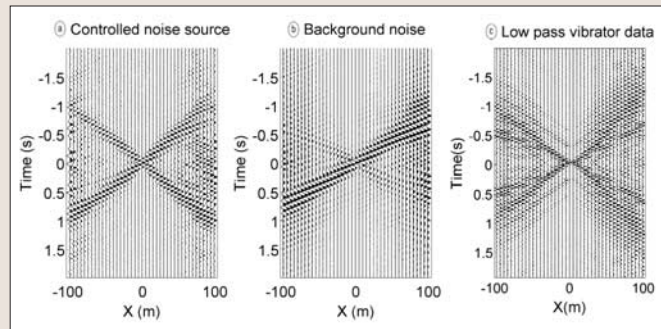


Figure 17. Time-offset equivalents of Figures 16b and d.

Vascelonos et al. (2007) who apply a similar technique to active source data).

We repeat the estimation process using the isolated noise, resulting in the surface wave estimates shown in Figure 15. The surface waves are clearer, but the spurious event can still be seen in the controlled noise source plot and faintly in the uncontrolled noise plot.

Since the unwanted noise is coming from the broadside of the receiver array, it will plot close to the zero wavenumber axis in *f-k* space, and hence can be suppressed using an *f-k* filter as the (direct) surface waves will not occur in the same region. Figure 16a and c show the data in Figure 13a and b in *f-k* space, and Figure 16b and d show the *f-k* plots after filter application (note that this type of filtering is not desirable when we are interested in near surface scattering, since it also suppresses any cross-line scattered surface waves). The equivalent time/distance plots are shown in Figure 17; the unwanted arrival is not visible in either the controlled noise data or the industrial noise data, while the estimate of the direct Rayleigh wave remains. Note that for the passive noise, there is also an event propagating in the opposite direction. This is not recovered in the beam forming approach. Since this arrival (and hence the source of noise) is weak, the noise from the building site was dominant, and the noise was not detected during directional analysis.

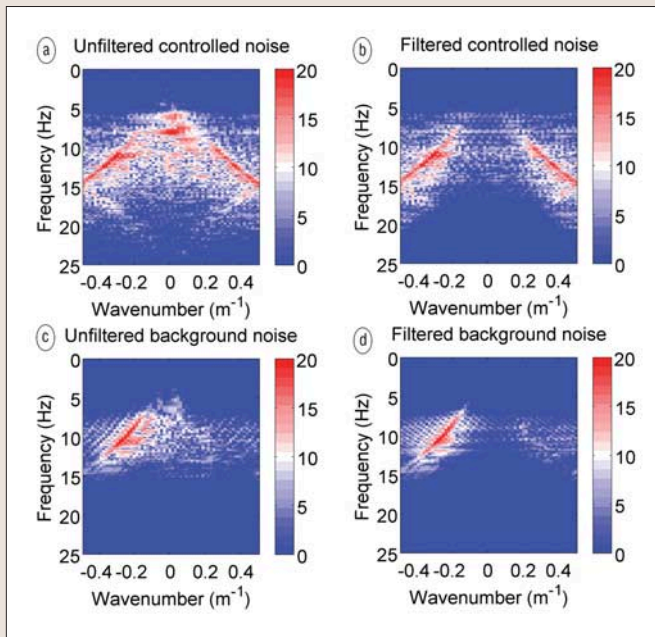


Figure 18. f - k plots (after directional analysis) for (a) controlled noise interferometric data, (b) f - k filtered controlled noise interferometric data, (c) unfiltered background noise interferometric data, and (d) f - k filtered background noise interferometric data.

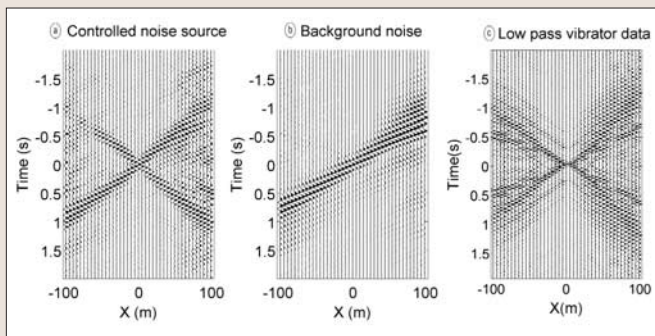


Figure 19. Time-offset equivalent of Figures 18b and d.

We combine both of these filtering processes with results shown in Figure 18 and Figure 19. Note that the weak event identified in Figure 17b is not seen in Figure 19b (or the equivalent f - k plot in Figure 18b), confirming that the directional filtering does not preserve this arrival. However, the estimates produced using both this directional approach and f - k filtering are affected less by artifacts (compare the regions at longer offsets around the zero-time axes in Figure 17 and Figure 19). These artifacts are likely to be introduced by other offline noise sources that are not cancelled in the interferometric summation, but which can be eliminated using the target-orientated approach.

The results illustrate that by applying passive seismic interferometry, we can extract inter-receiver surface wave signals, even when recording times are short and there is poor azimuthal coverage of background noise sources (typical of a suburban area). This results in estimates that are dominated by uncanceled, nonstationary phase sources. By applying some simple processing steps to both the passive noise records and the interferometric estimates themselves, we can nevertheless extract reasonable estimates of the surface waves.

Discussion and conclusions. We have shown that it is pos-

sible to use seismic interferometry to extract estimates of inter-receiver surface waves in a suburban setting. Active sources allow multimode surface wave data to be estimated with a bandwidth similar to that acquired in active surveys. Lower-frequency surface-wave estimates are extracted from recordings of background noise (excited by a controlled, continuous-noise source and random background sources), but these estimates are of lower quality than those from active sources (at least for the short recording periods used here).

In the passive case, the use of relatively short recording intervals and nonhomogeneous directionality of the noise sources results in problems due to cross-correlation contributions that do not correspond to real inter-receiver signals. To overcome these problems we use target-orientated passive interferometry and f - k filtering to enhance the estimates of the inter-receiver surface waves. Since our ability to estimate surface waves passively is controlled by the availability of noise sources it may be desirable to plan such surveys around prior knowledge of the noise. Receivers can be aligned such that noise sources lie in stationary regions for the inter-receiver surface waves. For example, in the above it may have been beneficial to have a second line of receivers perpendicular to the current array, since this line would have a stationary phase region coinciding with the busy motorway and building site.

One of the benefits of seismic interferometry is that source-receiver data can be estimated without active sources, or with only a few carefully located active sources. We have shown that interferometry can be used to acquire surface wave data sets equivalent to those recorded in more costly active source near surface surveys.

Comparing the different surface wave measurements we observe that the surface waves estimated using active-source interferometry have a broader frequency band than those in the real active data. This frequency difference is likely to be due to the differing receiver response functions of the two geophone types used (for the active vibrator sources, a highly damped geophone must be used to record the source wavelet, which is not necessary in the active source interferometric case). This is therefore a side effect of the acquisition equipment, and by using interferometry we can recover surface waves for a broader range of frequencies. A wider range of frequencies allows a greater range of depths to be studied with the data. Secondly, the passively estimated surface waves have lower frequency content than both the active-source interferometry and the real active data (e.g. Figure 11 and Figure 19). This presents the possibility of combining the active and passive methods to allow an even wider frequency range to be used when determining subsurface velocity from surface-wave data. Park et al. (2007) propose a similar combination of active and passive recordings using the multichannel analysis of surface waves (MASW) technique. However, they apply their method directly to the recorded noise as opposed to using an interferometric approach as presented here.

The application of the passive method is common in earthquake seismology but applications on the small scale presented here are rare. However, successful application can provide valuable information about the near surface without the use of dense source distributions. This approach may find applications in near-surface characterization in exploration environments, or in engineering geophysics.

Halliday and Curtis (2008) show theoretically and with synthetic examples that the use of certain geometries introduces spurious events in interferometric estimates of surface waves, and they propose modal separation as a solution to this problem. However, they find that inline geometries,

such as those presented above, allow for the recovery of surface waves propagating approximately in the inline direction without the introduction of any strong spurious events.

In areas with strong near surface heterogeneity, a similar approach may allow for the estimation of inter-receiver scattered surface waves, and therefore the analysis of near-surface scattering properties.

We are currently investigating the effects of source distribution in three dimensions and the potential of this method to recover scattered surface waves. We will apply similar methods to a 3D data set from a real setting displaying strong scattering of surface waves.

Suggested reading. "Seismic interferometry: Turning noise into signal" by Curtis et al. (*TLE*, 2006). "Seismic interferometry supplement" by Wapenaar et al. (*GEOPHYSICS*, 2006). "Interferometric prediction and least squares subtraction of surface waves" by Dong et al. (*SEG 2006 Expanded Abstracts*). "On interferometric surface wave (ground roll) isolation and removal" by Halliday et al. (*GEOPHYSICS*, 2007). "Space and time spectra of stationary stochastic waves with special reference to microtremors" by Aki (*Bulletin of the Earthquake Research Institute*, 1957). "Faster, better: Shear-wave velocity to 100 meters depth from refraction microtremor analysis" by Louie (*Bulletin of the Seismological Society of America*, 2001). "On the correlation of seismic microtremors" by Chávez-García and Luzón (*Journal of Geophysical Research*, 2005). "Inversion of source-generated noise in high-resolution seismic data" by Roth and Holliger (*TLE*,

1999). "Multichannel analysis of surface waves (MASW): Active and passive methods" by Park et al. (*TLE*, 2007). "Retrieval of reflections from seismic background-noise measurements" by Draganov et al. (*Geophysical Research Letters*, 2007). "Green's function representations for seismic interferometry" by Wapenaar and Fokkema (*GEOPHYSICS*, 2006). "Spurious multiples in seismic interferometry of primaries" by Snieder et al. (*GEOPHYSICS*, 2006). "Arrival-time structure of the time-averaged ambient noise cross-correlation in an oceanic waveguide" by Sabra et al. (*Journal of Acoustical Society of America*, 2005). "Minisose for shallow land seismology" by Barbier et al. (*Geophysical Prospecting*, 1976). "Target-oriented interferometry—Imaging with internal multiples from subsalt VSP data" by Vasconcelos et al. (*SEG 2007 Expanded Abstracts*). "Extracting the Green's function from the correlation of coda waves: A derivation based on stationary phase" by Snieder (*Physical Review E*, 2004). "Seismic interferometry, surface waves, and source distribution" by Halliday and Curtis (*Geophysical Journal International*, in press.) **T|E**

Acknowledgements: The authors thank the staff at Schlumberger Cambridge for their support of David Halliday during this work. We especially thank David Leslie, whose valuable assistance in the field aided timely completion of data acquisition. We also thank reviewer Roel Snieder for his useful comments.

Corresponding author: s0198946@sms.ed.ac.uk